Multifunctional Nanorods Serving as Nanobridges To Modulate T Cell-Mediated Immunity

Young Ju Son,[†] Hyesung Kim,[†] Kam W. Leong,[‡,§] and Hyuk Sang Yoo[†,⊥,*]

[†]Department of Biomaterials Engineering, Kangwon National University, Chuncheon 200-701, Republic of Korea, [‡]Department of Biomedical Engineering, Pratt School of Engineering, Duke University, Durham, North Carolina 27709, United States, [§]King Abdulaziz University, Jeddah, Saudi Arabia, and [⊥]Institute of Bioscience and Bioengineering, Kangwon National University, Chuncheon 200-701, Republic of Korea

ABSTRACT Electrodeposited nanorods serving as multivalent bridges were fabricated and surface-decorated with ligands for immune cells. Gold and nickel solutions were sequentially electrodeposited on nanoporous anodized disc templates and the template was dissolved to retrieve bisegmented nanorods with different lengths. Gold and nickel segmented nanorods were surface-immobilized with mannose and RGD peptides to prepare immune-cell recruiting nanorods. Surface-functionalization of nanorods were confirmed by fluorescence-labeling of each ligands and confocal microscopy. Dendritic cells and T cells were co-incubated with the surface-functionalized nanorods, and the proximity between the nanorods and the immune cells was visualized by variable pressure scanning electron microscopy and confocal microscopy. The long nanorods were associated with the immune cells, whereas the shorter nanorods were rather endocytosed by cells, suggesting a feasibility of the longer nanorods as bridging for the cells. Cytokine releases from the immune cells were monitored by cultivating lipopolysaccharide-activated dendritic cells with T cells. Interleukine-2 and interferon-γ release profiles showed a strong correlation with the length of the nanorod, where the 4 μm nanorods induced the highest levels of cytokine release compared to 1 or 2 μm nanorods. Thus, we concluded that the proximity of the immune cells increased by bridging the immune cells with the nanobridging system, which subsequently increased cytokine release by facilitating the antigen presentation process.

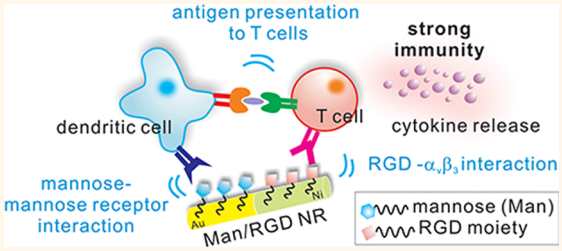

KEYWORDS: nanorods · antigen presentation · nanobridge · multifunctional · dendritic cell · T cell

Nanoparticle technology has long been applied to augment immunotherapy *via* effective delivery of antigen or immunoadjuvant to antigen presenting cells (APCs).[1−3] An interesting alternative approach is to use nanoparticles to activate or deactivate the surface receptors of APCs. For innate immunity, major histocompatibility complex (MHC) and foreign antigen on APCs are recognized by T cell receptors (TCR) on T cells, which is a critical step for antigen recognition. Thus, one immune modulating strategy is to decorate nanoparticles with immune cell-recognizable peptides, polysaccharides, and antibodies to enhance or intercept these MHC−TCR interactions, a strategy successfully demonstrated against infectious diseases and cancers.[4−6] For instance, short peptides containing MHC I or II covalently attached to carboxylated polystyrene beads could induce strong innate immunity and protection against tumor cell invasion by activating the antigen presentation pathway.[7] In another study, T cell-mediated immune response could be down-regulated by simultaneous blocking of lymphocyte function-associated antigen-1 (LFA-1) and intracellular adhesion molecule-1 (ICAM-1), accomplished by using two separate anti-LFA-1 and anti-ICAM-1 nanoparticles for dendritic cells and T cells, respectively.[8]

Spherical nanoparticles have been used in these studies. We hypothesize that multisegmented nanorods would be advantageous over spherical nanoparticles in engaging cell−cell interactions because of the spatial control of multiple ligands on a nanorod. Multisegmented metallic nanorods can be readily synthesized by templated electrodeposition. The diameter and length of the nanorods can be controlled by the template, typically a porous polymeric membrane that is removed by acid dissolution after the electrodeposition. Importantly, different

* Address correspondence to hsyoo@kangwon.ac.kr.

Received for review June 27, 2013 and accepted October 2, 2013.

Published online October 02, 2013
10.1021/nn403275p

metals can be deposited on the template in a sequential manner to create multiple segments of controllable length. This in turn allows different functional groups to be immobilized on the respective segments based on specific metal−ligand interactions, for example, thiol on Au and carboxylic acid on Ni. This strategy has been applied to improve biolistic gene gun delivery, with DNA immobilized on the Ni segment and transferrin on the Au segment of a bisegmented Ni/Au nanorod. It has also been used to functionalize triple-segmented nanowires composed of Au/Pt/Au with proteins through specific covalent linkages between proteins and metal segments.[9] We previously surface-functionalized bimetallic nanorods with a folate and a thermo-sensitive polymer for temperature-responsive incorporation and release of doxorubicin. Upon increasing the length of the gold segment where doxorubicin was immobilized, anticancer effect was accordingly escalated, highlighting the versatility to control the functionality of the nanorod by varying the length ratio of the metallic segments.[10] Thus, in terms of conferring multifunctionality and multivalency to nanostructures, multisegmented nanorods are superior to spherical nanoparticles because of the spatial control for heterogeneous surface chemistries.

We here propose a bridging strategy for facilitated T cell-mediated immune responses by increasing intercellular association of immune cells with immune-recognizable Au/Ni nanorods (Au/Ni NRs). Au/Ni NRs were fabricated by an electrodeposition technique, and the Au segment was surface-decorated with mannose, intended to target dendritic cells (DCs), and the Ni segment with a RGD peptide for immune cell recognition, respectively. By bridging DCs to T cell, we speculate the antigen presenting pathway will be facilitated due to the intercellular proximity, which is a critical step toward antigen presentation. Multifunctionalization of the nanorod was characterized by electron and confocal microscopy, and the cytokine release patterns from T cells were compared according to the segmental ratio of the functionalized nanorods. The proximity of the immune cells and the nanorods was also confirmed by electron microscopy and confocal microscopy. The *in vitro* T cell response as manifested by IL-2 and IFN-γ was enhanced with a Au/Ni ratio of *x*:*y* in the nanorods that were *x* nm in diameter and *y* μm in length.

RESULTS AND DISCUSSION

To fabricate an immune-recognizable 'nanobridge', a bisegmented nanorod composed of gold and nickel was electrodeposited and then surface-functionalized with two different ligands for bone marrow-derived dendritic cell (BMDCs) and Jurkat cells (Figure 1). The template-based fabrication of metallic nanorods by electrodeposition has several advantages such as multisegmentation of the nanorods and controlling the aspect ratio of the nanorods according to the electric Coulomb. Thus, we fabricated three types of bimetallic nanorods with different lengths (1, 2, and 4 μm) and then selectively surface-modified them with α-D-mannopyranosylphenyl isothiocyanate and GRGDS (Man/RGD NRs). This was accomplished by introducing thiol groups and carboxylate groups to poly(ethylene glycol) (PEG)ylated α-D-mannopyranosylphenyl isothiocyanate (mannose) and GRGDS (RGD moiety), respectively, for metal-selective immobilization and the synthesis of the conjugates were also confirmed (Figure 1A; Figure S1). PEGylation efficiency of mannose and RGD moiety was obtained to 82.17 and 89.50% (mol/mol), respectively, based on integral value of proton nuclear magnetic resonance (^{1}H NMR) spectroscopy. We also determined the PEGylation efficiencies for mannose and RGD moiety by reverse phase high-performance liquid chromatography system (RP-HPLC) so that unconjugated and conjugated PEG can be separated. For mannose, the native peaks of PEG shifted from 22.6 to 45.1 min due to the conjugation with a significant decrease of the native PEG peak (Figure S2). By comparing the peak areas of the native PEG and the mannose at 22.6 min, the amount of mannose in the conjugate was confirmed to 82.86%, which well coincides with the results from NMR spectroscopy (82.17%). Likewise, the amount of RGD moiety in the reaction mixture was confirmed to be 51.13%. The PEGylation, served as a spacer to ensure a good display of the ligand on the surface, and to improve the colloidal stability of the nanorods. Because the ligands were displayed on the surface *via* a hydrophilic linker, we speculated that the ligands could be easily recognizable by immune cells as shown in the literature.[11,12] Additionally, we restricted the size of PEG to be 2.0−3.4 kDa because we need to minimize the antifouling effects of the decorated PEGs toward the immune cells. Thus, this can cause slight increase of the aggregation behaviors of the decorated nanorods considering that many nanosized particles are extensively decorated with the large PEG molecules to prevent the aggregation of the particles.[13−16]

Numerous studies have indicated that thiolated molecules and carboxylated biomolecules could be selectively immobilized on the surface of Au and Ni through these linkages.[10,17] Previously, we fabricated bimetallic nanorods by electrodeposition and selectively surface-functionalized the Au/Ni segments with thiolated Pluronic and folate.[10] Here, the metal selective-decoration strategy of bimetallic nanorods was employed for fabricating immune-recognizable nanobridges. Thus, the decorated nanorods made of equal part of RGD moieties and mannose show a multivalency toward BMDCs and Jurkat cells (Figure 1B and C). Antigen presentation occurs when antigen presenting cells such as mature and activated dendritic cells are in close contact with immature T cells to present a MHC and peptide fragment complex to TCR and activate T cells. Thus, we speculate that the antigen presentation

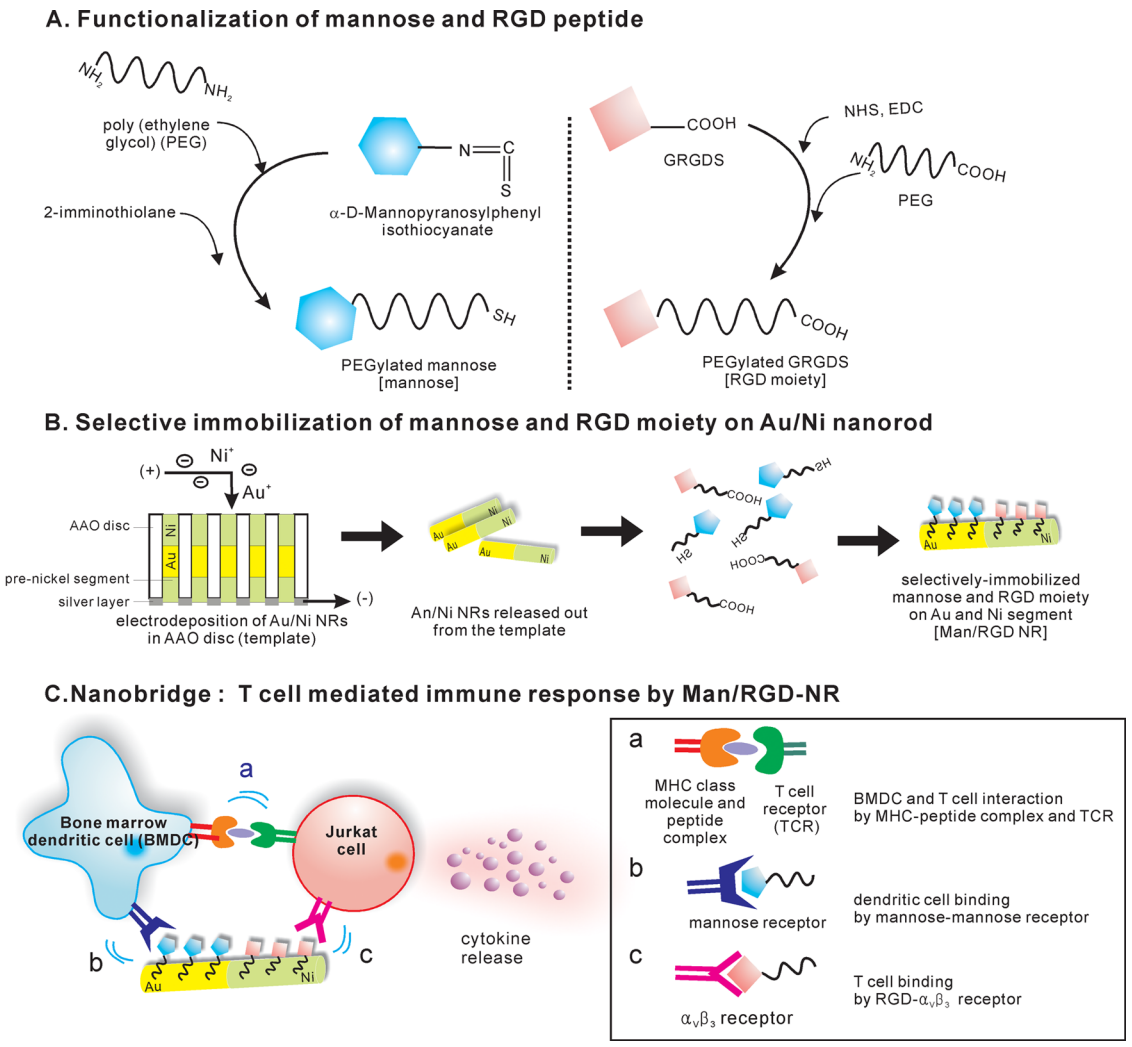

Figure 1. Preparation of Au/Ni nanorod for selective immobilization of mannose moiety and GRGDS (Man/RGD NR) and description of 'nanobridge' for enhanced T cell-mediated immune responses. (A) Functionalization of mannose and RGD moiety for surface-immobilization. After PEGylation of α-D-mannopyranosylphenyl isothiocyanate, the terminal amine group of PEGylated mannose was thiolated with 2-imminothiolane. PEGylated GRGDS (RGD moiety) was synthesized by conjugating heterofunctional PEG (NH_2-PEG-COOH) to the activated GRGDS peptides. (B) Selective immobilization of Au and Ni segments with the functionalized mannose and RGD moieties. After sequential electrodeposition of Au and Ni, mannose and RGD moiety were added for selective modification by Au-thiol and Ni-carboxylic acid reactions. (C) BMDC and Jurkat cell-recognizable 'nanobridge' for facilitating antigen presentation. By bridging between BMDC and Jurkat cell, the antigen presentation is facilitated and T cell mediated immune response is fortified.

behavior can be greatly influenced by the proximity of those two cells. We also hypothesize that the antigen presentation event of two immune cells can be controlled by changing the segmental lengths of the dual-functionalized nanobridge because those interactions can be facilitated or suppressed according to the manipulated proximity.

After fabricating bimetallic nanorods with two different ligands, we confirmed the Au/Ni NR structure and spatially controlled immobilization of RGD and mannose moieties on the nanorods by scanning electron microscopy (SEM) and confocal scanning laser microscopy (CLSM) (Figure 2). The backscattered SEM images clearly showed that the nanorods were composed of Au (light gray) and Ni (dark gray) segments with a 1:1 aspect ratio and the total length was 1, 2, and 4 μm (Figure 2A). When the surface-immobilized ligands were fluorescently labeled with respective dyes, the mannose moieties and RGD moieties were confirmed to be spatially confined on the Au/Ni NRs, maintaining the same aspect ratio of Au/Ni NRs (Figure 2B). This result clearly confirmed that those ligands were selectively attached to each segment; the mannose moieties to Au segments and the RGD moieties to Ni segments. We did not perform additional purification steps during the preparation of the mannose- or RGD-conjugated PEGs because of the high conjugation efficiency of each ligand to the PEG conjugates as well as the nonimmunogenic property of PEG molecules.[18,19] As shown in Figure 2C, while the mannose moieties and the RGD moieties were immobilized on the surface at the same aspect ratio (1:1),

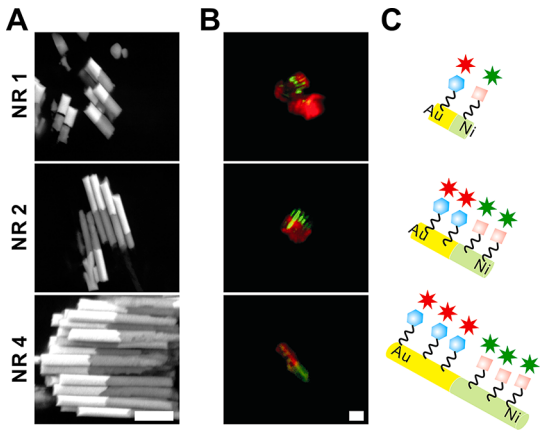

Figure 2. Visualization of Man/RGD NR with different lengths (NR 1 = 1 μm, NR 2 = 2 μm, and NR 4 = 4 μm). Backscattered SEM images (A) shows bisegmented nanorods composed of Au (white) and Ni segment (dark gray) of fluorescently labeled Man/RGD NR. In CLSM images (B), where Alexa 647-labeled mannose and FITC-labeled RGD moieties are shown in red and green, respectively. The illustrations of the Man/RGD NR are also represented (C). The scale bars of all microscopic images are 2 μm.

the functionalized area of the nanorods gradually increase as the length of the nanorods increase from 1 to 4 μm. Thus, we hypothesize that the Man/RGD NR would show multivalency against two different immune cells while the affinity toward respective cells would escalate as the length of the nanorods increases due to the increased amount of mannose moieties or RGD moieties on NR surface. Unlike spherical nanoparticles, the degree of surface-immobilization on the nanorods is readily controllable and favorably employed to surface-immobilize different ligands toward specific cell types in a single nanorod, whose implication on interactions with cells has been amply documented in the literature.[20−23]

Man/RGD NRs were incubated with Jurkat cells and differentiated BMDCs (as confirmed in Figure S2), and their proximity was visualized by variable pressure SEM (VP-SEM) with energy dispersive X-ray spectroscopy (EDX) and CLSM as shown Figure 3. We preincubated with Jurkat cells with Man/RGD NRs for 3 h prior to addition of BMDCs to maximize the RGD−$\alpha_v\beta_3$ interactions between the RGD moieties of the NRs. To monitor the association of NRs to Jurkat cells or BMDCs, we employed VP-SEM to capture the images of the cells associated with NRs. Although mannose and RGD moieties have high affinities toward respective receptors on cells, the associated NRs/immune cells complex might be disrupted during the preparation of specimen for conventional SEM due to harsh conditions such as dehydration or drying steps. During the preparation of samples for VP-SEM, however, the NRs associated with cells remained intact because the disruption could be minimized as discussed in the experimental. Thus, after placing the fixed NRs/immune cells complex on a cool stage of VP-SEM, we visualized the moment of cell-to-NR interactions in an identical status of *in vitro* cultivation. In Figure 3A,D,G, the VP-SEM images visualized the Man/RGD NRs association with immune cells at low and high magnification and the orientation of the NRs was also confirmed by elemental analysis, where the spotted nanorods were analyzed by EDX for confirmation of Ni (green spots) and Au (red spots) (Figure 3B,E,H). Most short nanorods were engulfed or phagocytosed by cells, while longer ones were surface-attached to the cells; NRs in NR 1 (Figure 3A) were buried in the cellular membranes while the morphology of the NRs became distinguishable from Man/RGD NR 2 (Figure 3D) to Man/RGD NR 4 (Figure 3G). This can be attributed to the differential phagocytic behaviors of cells depending on the dimension of NRs. Previous studies employing nanorods and nanowires with smaller dimensions have consistently indicated that small nanorods and nanowires have a tendency to be engulfed by surrounding cells.[16,24] In our previous study, we also observed that the bisegmented nanorods below 2 μm were internalized by cancer cells after ligand−receptor interaction in the cell surface, where the endocytic uptakes were desirable for delivery of anticancer drugs.[10] In another study, electrodeposited nanorods for gene therapy were employed for transfection of cancer cells. Due to the short length of 100 nm, the nanorods were efficiently endocytosed by the cells.[17] Although the efficiency of phagocytosis is dependent both on cell type and rigidity of the nanowire, the size has been shown to be the major factor controlling cellular uptake.[15,25−27] Similarly, in the current study, the tendency of phagocytosis clearly decreased when the size of the NR increased; we observed that some Man/RGD NR 2 was also phagocytosed, and Man/RGD NR 4 was not engulfed by cells. This result strongly suggests that the length of a nanobridge needs to be optimized to tether immune cells together for facilitated immune responses because the bridges are required to be located on the surface of the immune cells. Thus, we speculated that Man/RGD NR 4 can serve as the potential candidate for the nanobridge over Man/RGD NR 1 or Man/RGD NR 2 in terms of minimizing the cellular uptake.

Although the proximity of the immune cells to NRs could be visualized by SEM, this method could not confirm whether the bridging was actually caused by specific interactions between the immobilized ligands of NRs and respective cellular receptors. This was accomplished by tagging each molecule and cell with specific fluorescence probes and examination by CLSM. Figure 3C,F,I show the CLSM images of NR-immune cells complex, where Jurkat cell (blue) and BMDC (yellow) were fluorescently labeled for discrimination of cell types. Mannose (red) and RGD moieties (green) on the NRs were also labeled for determining their directions. In Figure 3C, Man/RGD NR 1 (white triangle) was located in the middle of BMDC in the 2-D view. This suggests that the NR 1 was internalized by

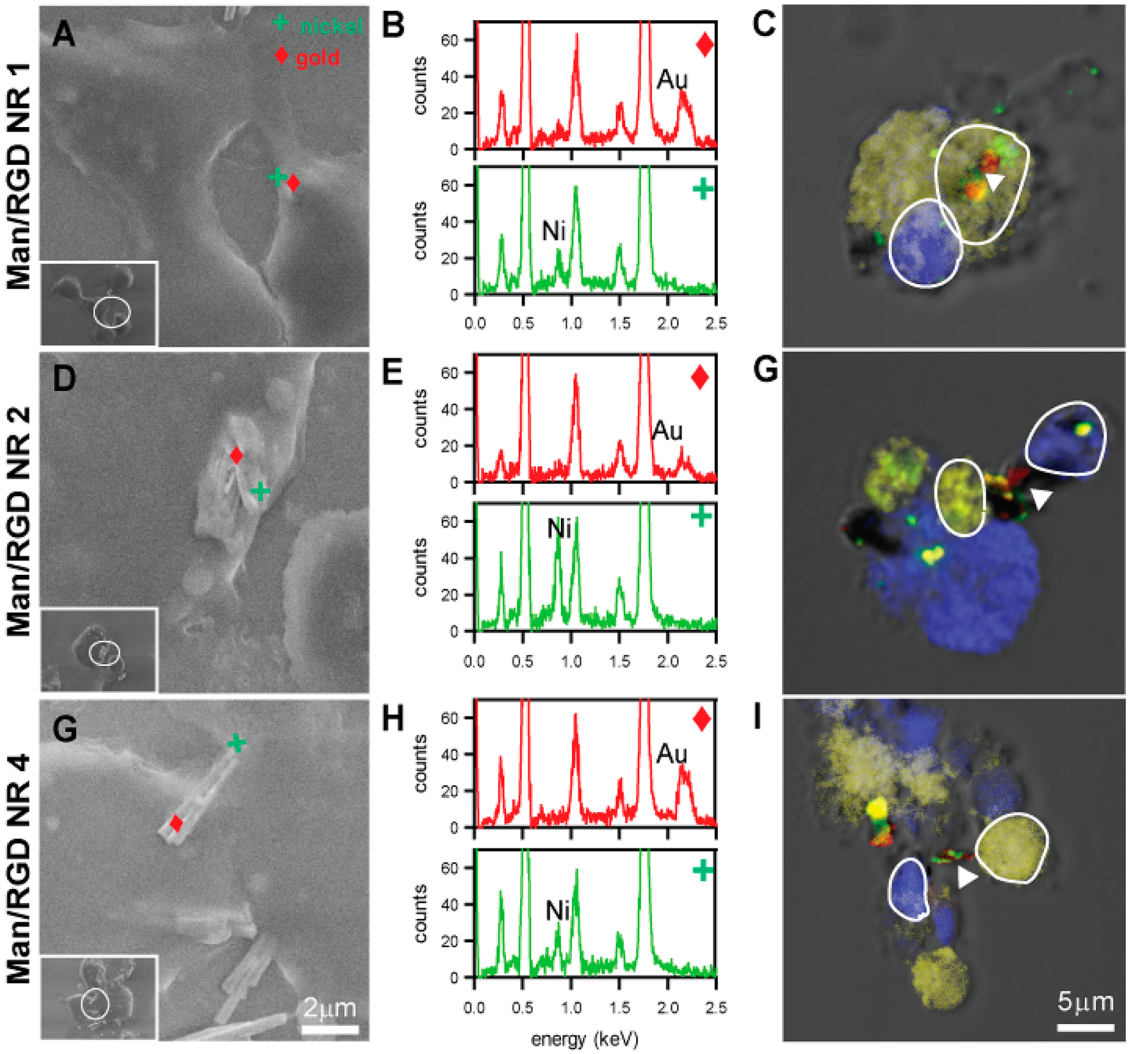

Figure 3. Visualization of the immune cells bridged with Man/RGD NRs. The proximity of the nanorods was confirmed both by VP-SEM (A, D, and G) equipped with EDX (B, E, and H) and CLSM (C, F, and I). Man/RGD NRs were incubated with T cells for 3 h and LPS-activated BMDCs were then added. After 18 h, Man/RGD NR associated with BMDC and T cell was visualized by VP-SEM on a cool-stage at −14 °C (left). While the inset images are in low magnification, the magnified images of the white circles in the inset were also shown. EDX spectrum of the indicated spots (♦/+) in SEM images (middle). The peaks of Ni (0.9 keV) and Au (2.3 keV) were assigned to determine the orientation of the mannose or RGD moiety. In CLSM images, BMDC (yellow) and Jurkat cell (blue) were shown with Man/RGD NR (white triangle (▽)) with RGD (green) and mannose (red) (right panel).

the cells rather than attached on the surface of the cells. However, Man/RGD NR 2 and Man/RGD NR 4 were shown to be attached on the surface of the cells and located between Jurkat cells and BMDCs. More specifically, the orientation of the NRs was dependent on the ligands−receptor interaction; the mannose (red) was attached to the surface of BMDCs (yellow) while the RGD moieties (green) were associated with Jurkat cells (blue). Together with the VP-SEM images, these results clearly suggest that the longer NRs can play a role of a bridge to tether Jurkat cells and BMDCs by the specific ligand−receptor interactions. Several studies have previously shown that immune responses could be stimulated with multivalent nanospheres.[25,28] The conventional immunotherapeutic strategies were mainly focused on increasing the avidity of the nanospheres by immobilizing multiple ligands and using the decorated nanospheres to subsequently block or stimulate the receptors for suppressing and provoking immune responses. On the other hand, our study is well distinguished from those studies in terms of the binding strategy; Man/RGD NRs are designed as nanobridges to simultaneously target toward multiple types of immune cells and bringing them together.

Cytokine release of T lymphocytes, a hallmark of humoral immunity, is primarily caused by antigen presentation of activated dendritic cells. We therefore monitored the cytokine levels to determine the effects of the nanobridging on the antigen presentation process. IL-2 and IFN-γ are representative cytokines by activated T lymphocytes that were evaluated to characterize antigen delivery efficiency by antigen encapsulated nanoparticle to APCs or T cell activation efficiency.[29,30] First, the ratio of the NRs to BMDCs was

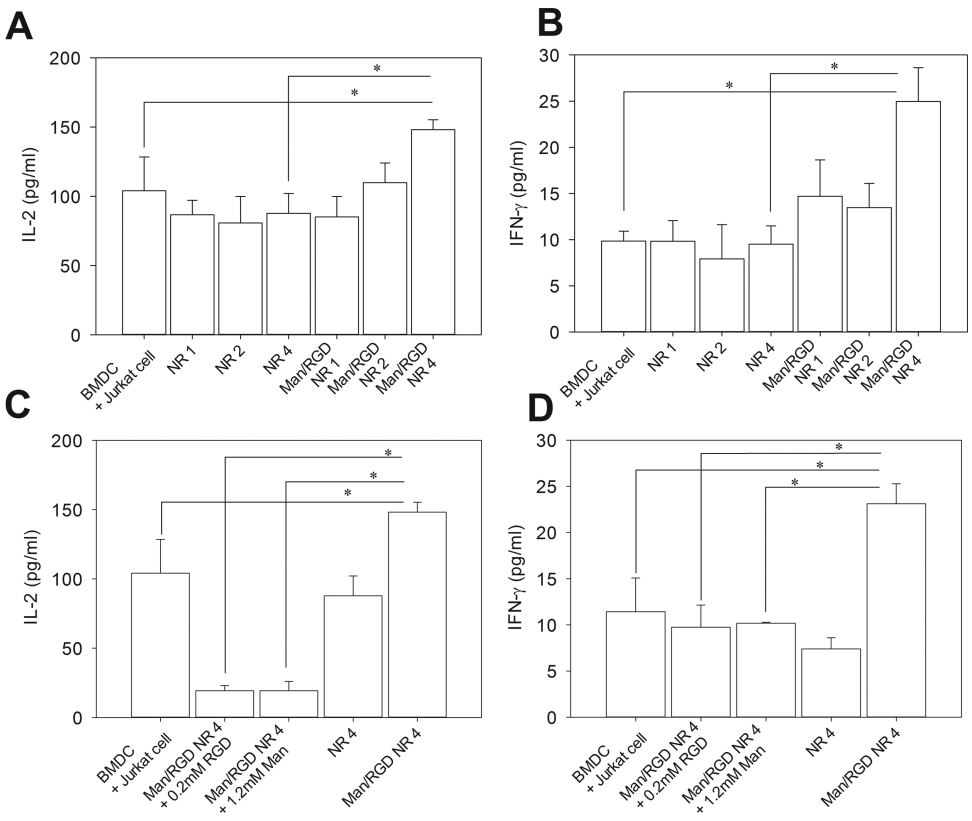

Figure 4. Cytokine release from T cell upon administration of nanorods. Jurkat cells were incubated with Man/RGD NRs at the presence of CD11c$^+$ BMDCs in serum free media for 24 h. Man/RGD NRs were preincubated with Jurkat cells for 3 h and CD11c$^+$ BMDCs were added (number ratio of NR/Jurkat cell/BMDC = 50:5:1). (A) Interleukine-2 (IL-2) and (B) interferon-γ (IFN-γ) levels of the released medium were determined by ELISA as described in Materials and Methods. In panels C and D, RGD receptor ($\alpha_v\beta_3$) on T cells or mannose receptors on BMDC were preblocked in the cell culture medium containing 0.2 mM GRGDS or 1.2 mM D-mannose to disturb the association of Man/RGD NR 4 toward immune cells. (C) IL-2 and (D) IFN-γ levels were measured with the same method. Asterisk (*) indicates statistical significance ($p < 0.05$).

optimized for increased levels of cytokine production. This was accomplished by escalating the number of NR with respect to that of Jurkat cells from 1 to 500 with a fixed ratio of BMDCs to Jurkat cell (Figure S3). We measured IL-2 levels for 24 h and concluded that a 50:1 ratio of NRs to Jurkat cells would be optimal because the cytokine production did not show significant improvement beyond this ratio. On the basis of the preliminary study, IL-2 and IFN-γ levels were determined for the bridging system composed of the immune cells and Man/RGD NRs with different lengths (Figure 4). The cytokine levels showed a strong dependency on the length of the NRs; the cytokine levels clearly increased when the length of the NR increased from NR 1 to NR 4 (Figure 4A,B). Up to 2 μm in length, the decorated NRs did not show any statistical differences in cytokine levels compared to unmodified NRs. However, Man/RGD NR 4 clearly increased both IL-2 and IFN-γ levels by 1.4- and 2.5-fold in comparison to those with NRs, respectively. Thus, we can speculate that all Man/RGD NRs can bind to the immune cells by specific ligand−receptor interactions; however, Man/RGD NR 1 and Man/RGD NR 2 cannot serve as nanobridges because they are internalized after the specific binding. In accordance with the result from Figure 3, this result strengthens the importance of the optimized length for the bridging system for facilitated antigen presentation.

Furthermore, we also inhibited the specific ligand−receptor interactions of Man/RGD NRs toward the immune cells to exclude the possibility of nonspecific activation of immune responses by gold segments as indicated by several studies (Figure 4C,D).[15] When either of RGD moiety or mannose was added to the bridging system, the cytokine levels were significantly diminished. This can be certainly attributed to the blocking of $\alpha_v\beta_3$ receptors and mannose receptor of Jurkat cells and BMDCs. In the bridging system, Man/RGD NRs need to be simultaneously anchored both to BMDCs and Jurkat cells for facilitation of antigen presentation. Thus, when either of this anchoring is blocked, the whole process of the antigen presentation is affected and the cytokine release is decreased accordingly. Because the cytokine levels of Man/RGD NRs groups were much higher even compared to Jurkat cells and BMDCs mixture without any nanorods, this result clearly suggests that surface-decorated nanorods can be served as bridges to tether two types of immune cell and the cytokine release was very dependent on

the length of the nanorods. The possibility of immune response by short peptide like RGD or mannose itself, gold, and PEG is subsequently excluded from many literatures.[4,15,19,25,31] Consequently, we herein proved that antigen presentation of DCs could be facilitated by the physical bridging of two immune cells, whose concept was proved by bisegmented nanorods codecorated with mannose and RGD moieties.

CONCLUSION

A novel application of multisegmented nanorods was demonstrated in this study to facilitate the antigen presentation process. Bisegmental Au/Ni nanorods, 1−4 μm in length and 300 nm in diameter, and selectively decorated with mannose and RGD moiety on the respective metallic segments, served as nanobridges to bring BMDC and Jurkat cells into close proximity. The 4 μm Au/Ni nanorods were optimal with respect to minimal phagocytosis and maximal enhancement of IL-2 and IFN-γ secretion. These novel nanorods may serve as interesting tools for ligand discovery toward immunotherapy and to gain mechanistic insight on the antigen presentation process.

MATERIALS AND METHODS

Materials. Anodized aluminum oxide (AAO) membrane, Anodisc, with a pore size of 0.1 μm, was obtained from Whatman (Maidstone, England). Nickel(II) sulfate hexahydrate, nickel(II) chloride, α-D-mannopyranosylphenyl isothiocyanate, lipopolysaccharide, and 2-mercaptoethanol were purchased from Sigma-Aldrich (St. Louis, MO). GRGDS (Anygen, South Korea) was purchased from Anygen (Gwangju, South Korea). Poly(ethyleneglycol) diamine (PEG-$(NH_2)_2$, M_w 2000) and amine-poly(ethyleneglycol)-acid (NH_2-PEG-COOH, M_w 2000) were purchased from Sunbio (Anyang, South Korea). Human T lymphocytes (Jurkat cell) were purchased from Korean Cell Line Bank (Seoul, South Korea). RPMI1640 medium, fetal bovine serum (FBS), streptomycin, penicillin, Trypsin/EDTA, and Alexa 647 conjugated concanavalin A were purchased from Invitrogen (Carlsbad, CA). Anti-CD11c (mouse), anti-CD3 (human), and human interferon gamma (IFN-γ) ELISA development kits (ELISA Ready-SET-Go) were purchased from eBioscience (San Diego, CA). Recombinant murine granulocyte macrophage-colony stimulating factor (GM-CSF) and human interleukin-2 (IL-2) ELISA development kit were purchased from Peprotech (Rocky Hill, NJ). FITC-anti CD11c (mouse) and FITC-IgG1 (hamster, isotype control) were purchased from BD Pharmingen (San Diego, CA). Alexa Fluor 405 carboxylic acid succinimidyl ester and Texas Red-X succinimidyl ester (mixed isomers) were purchased from Invitrogen.

Electrodeposition of Multisegmented Metallic Nanorod. Multisegmented metallic nanorods were electrodeposited on the nanoporous Anodisc with the same method as previously described in the literature with minor modifications.[17] Briefly, the aspect ratio of Au/Ni NRs was uniformly controlled by electrically depositing Au and Ni ions into porous Anodisc (template), where one side of the Anodisc was covered with silver layer by a thermo-evaporation technique (National Nanofab Center, Daejeon, Korea). Ni ions were first deposited to prevent 'mushroom effect' between gold segment[17] and then Au and Ni ions were sequentially deposited in order to fabricate Au/Ni multisegmented metallic nanorods. Reductive potential was applied at −0.95 V and a Coulomb charge was applied according to the length of Au or Ni segment (−1.3 to −3.8 C or −1.4 to −6.9 C). To release individual Au/Ni NRs from the template, silver layer and pre-Ni segment were dissolved in 70% (v/v) nitric acid solution and Anodisc was dissolved in 3 M sodium hydroxide. Au/Ni NRs were washed with methanol several times and visualized with a back scattered field emission scanning electron microscope at the Central Laboratory of Kangwon National University (FE-SEM, S-4300, Hitachi, Japan).

Synthesis of Mannose and GRGDS for Immobilization. Mannose and GRGDS were immobilized on Au and Ni segment through a short spacer of PEG, respectively. α-D-Mannopyranosylphenyl isothiocyanate (2 mg) in methanol (1 mL) was slowly added to PEG-$(NH_2)_2$ (10.62 mg) in methanol (10 mL). The reaction mixture was reacted at 4 °C for 12 h and vacuum-dried at 30 °C. Then, another amine at the end of the PEG was thiolated with Traut's reagent (5.8 mg) in 50 mM bicine buffer (10 mL, pH 8.0), at 4 °C for 1 h and dialyzed in distilled water (DW) three times (Spectra Por 6, MW cutoff = 1000). To PEGylate GRGDS (RGD moiety), the C-terminus of GRGDS (1 mg) was activated using EDC (0.38 mg) and NHS (0.66 mg) in 0.1 M bicine buffer (pH 8.5) (the molar ratio of GRGDS/EDC/NHS = 1:10:2.69) to prevent any tail−head polymerization, and subsequently reacted with NH_2-PEG-COOH (5.66 mg) at 4 °C for 12 h. Unreacted GRGDS and chemicals were removed by extensive dialysis in DW (SpectraPor6, MW cutoff = 1000). PEGylated mannose was characterized by 600 MHz ^{1}H NMR spectroscopy in dimethyl sulfoxide-d_6 (DPX600, Bruker). The purities of PEGylated mannose and PEGylated RGD were determined by reverse phase high-performance liquid chromatography system (RP-HPLC, UltiMate3000, Dionex) equipped with a C18 column (250 × 4.6 mm, 5 μm, 300 Å, Jupiter). Mobile phase of DW/methanol or acetonitrile gradient (1−30% in 30 min) was employed at 0.6 mL/h and the signals were detected at 220 nm.

Surface-Modification of Au/Ni NRs with Mannose and RGD Moiety. The Au segment and the Ni segment were exclusively decorated with mannose and RGD moiety, respectively. To immobilize Man on Au segments, nanorod suspension (0.01−0.80 mg) in methanol was mixed with Man (0.08−0.32 mg) as the molar ratio of Au to Man was 1:1, under strong shaking at room temperature for 2 h. Sequentially, RGD moiety (0.2−0.8 mg) was added to the nanorod suspension and reacted at 4 °C for 12 h. Unmodified mannose and RGD moiety and were washed out with distilled water (DW) 10 times. To confirm specific immobilization of mannose and RGD moiety on Au/Ni NRs (Man/RGD NRs), mannose and RGD moiety were fluorescently labeled with Alexa 647 conjugated concanavalin A (Alexa 647-Con A) and fluorescence isothiocyanate (FITC). Alexa 647-Con A (200 μg/mL) was specifically bound to Man on Au segment in PBS (pH 7.2) at room temperature for 3 h and FITC was chemically conjugated with N-terminal of GRGDS on Ni segment in methanol at 4 °C for 12 h. Excessive amounts of fluorescent dye were washed out with PBS and methanol and visualized by confocal scanning laser microscopy (CLSM) at Korea Basic Science Institute (Carl Zeiss, LSM700, Germany). Alexa 647-ConA and FITC were individually excited at 633 nm (helium−neon laser) and 488 nm (argon-ion laser). Emission filters were set for detection of Alexa 647 (bp 620−680 nm) and FITC (bp 520−540 nm) at multitracking modes.

Preparation of BMDCs. Lymphocytes from murine bone marrow were freshly prepared and differentiated into BMDC by GM-CSF with a minor modification according to the literature.[26] Bone marrow cells (5 × 10^5 cell/mL) from the femurs and the tibia of C57BL/6 mice (female, 5−8weeks) were seeded on a bacteriological plate and cultivated in 10 mL of a dendritic cell-differentiation medium (R10) with 200 U/mL of GM-CSF (R10; RPMI supplemented with 10% FBS (v/v), streptomycin/penicillin, and 50 μM of 2-mercaptoethanol). At day 3, 10 mL of additional fresh R10 containing 200 U/mL of GM-CSF was added to the plate. At day 6 and 8, the half media was exchanged with fresh R10 containing 100 U/mL of GM-CSF. To quantify the amount of $CD11c^+$ BMDCs, the nonadherent cells at day 7 or 8 were collected and washed with PBS and resuspended in an

immunostaining buffer (PBS, 0.1% (v/v) FBS, 0.1% (v/v) sodium azide) in a round-bottom tube. Cells were fluorescently labeled with FITC-anti-CD11c at 4 °C for 20 min and $CD11c^+$ BMDCs were analyzed by flow cytometry (FACSCalibur, BD Biosciences, San Jose, CA). Cells with desirable forward scattering and side scatting intensities between 200 and 700 were gated and further analyzed for detection of FITC-anti-CD11c labeled cells by Cell Quest Pro software (λ_{ex} = 488 nm; λ_{em} = 525 nm band-pass filter (bp)). After confirming $CD11c^+$ BMDCs at day 7 or 8, the cells were activated and matured with R10 with 30 U/mL GM-CSF containing 1 μg/mL lipopolysaccharide for 24 h.

Bridging of BMDCs and Jurkat Cells *via* Man/RGD NRs. T cell-mediated immune response *via* Man/RGD NRs was investigated according to different ratios or lengths of Man/RGD NRs. Jurkat cell were plated on 24-well cell culture plates and serum-free media was fed (1×10^5 cells). After 1 h, different amounts of Man/RGD NRs (length = 1, 2, and 4 μm; NR 1, NR 2, and NR 4) were added and further incubated in 5% CO_2 at 37 °C for 3 h. The LPS-activated $CD11c^+$ BMDCs in serum-free media (2×10^4 cells) were added. After 21 h of cultivation, IL-2 and IFN-γ level secreted from the Jurkat cells were measured by ELISA at 3 and 24 h according to the manufacturer's protocol. To confirm specific ligand−receptor interactions, mannose receptors on BMDC were blocked in 1.2 mM D-(+)-mannose for 15 min and RGD receptors ($\alpha_v\beta_3$ integrin) of Jurkat cells were blocked by 0.8 mM GRGDS just before the bridging study.

Visualization of the Bridging System. To visualize bridging of Jurkat cell and BMDCs *via* Man/RGD NRs, Man/RGD NRs, Jurkat cell, and BMDCs were fluorescently labeled and monitored by CLSM and SEM. Jurkat cell in serum-free media (1×10^5 cells/mL) was dropped on a poly-L-lysine-coated glass and fluorescently labeled Man/RGD NRs suspension in PBS (2 μg/mL). After the 1 h incubation, BMDCs in serum-free media (1×10^5 cells/mL) were added and the mixture was incubated for 12 h (BMDC/Jurkat cell/NR = 1:1:10). Fluorescence labeling of anti-CD11c and anti-CD3 antibodies with Alexa Fluor 405 carboxylic acid succinimidyl ester and Texas Red-X succinimidyl ester was performed according to the manufacturer's labeling protocol for proteins. For immunofluorescence staining, cells were blocked with a blocking buffer (10% FBS, 0.09% sodium azide in PBS) for 1 h at 4 °C and labeled with Alexa 405-anti CD11c (2.5 μg/mL) and Texas Red-anti CD3 (2.5 μg/mL) in immunostaining buffer for 1 h at 4 °C, respectively. Cell were fixed with 2.5% (v/v) *p*-formaldehyde for 15 min and washed with PBS. Fluorescently labeled Man/RGD NRs, Jurkat cell, and BMDCs were visualized by CLSM. Texas Red labeled BMDCs and Alexa 405 labeled Jurkat cells were individually excited at 532 and 405 nm, and the emission signals were detected at bp 600−650 and 420−470 nm. FITC and Alexa 647 labeled RGD and Man were excited and emitted with the same condition of Man/RGD NRs' visualization by CLSM. Variable Pressure SEM (VP-SEM) was employed to minimize dissociation of NRs from the immune cells during the sample preparation according to the literature.[27] Briefly, Man/RGD NRs, Jurkat cells, and BMDCs on a cover glass were fixed with 2.5% (v/v) *p*-formaldehyde for 20 min and washed. Cells were placed in a closed chamber for 1 h, where osmium tetroxide solution (1%, w/v) was vaporized. The stained cells and their proximity with Man/RGD NRs were visualized on cool stage at −14 °C with VP-SEM and energy-dispersive X-ray spectroscopy (EDX) of the nanorods was obtained (Carl Zeiss, Supra 55VP, Germany).

Conflict of Interest: The authors declare no competing financial interest.

Acknowledgment. This work was supported by the Ministry of Health and Welfare and in Korea (2012-A120660) and the National Research Foundation in Korea (NRF-2012R1A2A2A01005857).

Supporting Information Available: Additional figures of ^{1}H NMR, reversed phase chromatography, flow cytometry, quatification of IL-2 from Jurkat cells. This material is available free of charge *via* the Internet at http://pubs.acs.org.

REFERENCES AND NOTES

1. Kwon, Y. J.; Standley, S. M.; Goh, S. L.; Fréchet, J. M. J. Enhanced Antigen Presentation and Immunostimulation of Dendritic Cells Using Acid-Degradable Cationic Nanoparticles. *J. Controlled Release* **2005**, *105*, 199–212.
2. Cui, Z.; Han, S. J.; Vangasseri, D. P.; Huang, L. Immunostimulation Mechanism of Lpd Nanoparticle as a Vaccine Carrier. *Mol. Pharmaceutics* **2005**, *2*, 22–28.
3. Nembrini, C.; Stano, A.; Dane, K. Y.; Ballester, M.; van der Vlies, A. J.; Marsland, B. J.; Swartz, M. A.; Hubbell, J. A. Nanoparticle Conjugation of Antigen Enhances Cytotoxic T-Cell Responses in Pulmonary Vaccination. *Proc. Natl. Acad. Sci. U.S.A.* **2011**, *108*, E989–E997.
4. Kim, T. H.; Jin, H.; Kim, H. W.; Cho, M. H.; Cho, C. S. Mannosylated Chitosan Nanoparticle-Based Cytokine Gene Therapy Suppressed Cancer Growth in Balb/C Mice Bearing Ct-26 Carcinoma Cells. *Mol. Cancer Ther.* **2006**, *5*, 1723–1732.
5. Yoshikawa, T.; Okada, N.; Oda, A.; Matsuo, K.; Matsuo, K.; Mukai, Y.; Yoshioka, Y.; Akagi, T.; Akashi, M.; Nakagawa, S. Development of Amphiphilic Γ-Pga-Nanoparticle Based Tumor Vaccine: Potential of the Nanoparticulate Cytosolic Protein Delivery Carrier. *Biochem. Biophys. Res. Commun.* **2008**, *366*, 408–413.
6. Akagi, T.; Wang, X.; Uto, T.; Baba, M.; Akashi, M. Protein Direct Delivery to Dendritic Cells Using Nanoparticles Based on Amphiphilic Poly(Amino Acid) Derivatives. *Biomaterials* **2007**, *28*, 3427–3436.
7. Fifis, T.; Mottram, P.; Bogdanoska, V.; Hanley, J.; Plebanski, M. Short Peptide Sequences Containing MHC Class I and/or Class II Epitopes Linked to Nano-Beads Induce Strong Immunity and Inhibition of Growth of Antigen-Specific Tumour Challenge in Mice. *Vaccine* **2004**, *23*, 258–266.
8. Chittasupho, C.; Shannon, L.; Siahaan, T. J.; Vines, C. M.; Berkland, C. Nanoparticles Targeting Dendritic Cell Surface Molecules Effectively Block T Cell Conjugation and Shift Response. *ACS Nano* **2011**, *5*, 1693–1702.
9. Wildt, B.; Mali, P.; Searson, P. C. Electrochemical Template Synthesis of Multisegment Nanowires: Fabrication and Protein Functionalization. *Langmuir* **2006**, *22*, 10528–10534.
10. Park, S.; Son, Y. J.; Leong, K. W.; Yoo, H. S. Therapeutic Nanorods with Metallic Multi-Segments: Thermally Inducible Encapsulation of Doxorubicin for Anti-Cancer Therapy. *Nano Today* **2012**, *7*, 76–84.
11. Blume, G.; Cevc, G.; Crommelin, M. D. J. A.; Bakker-Woudenberg, I. A. J. M.; Kluft, C.; Storm, G. Specific Targeting with Poly(Ethylene Glycol)-Modified Liposomes: Coupling of Homing Devices to the Ends of the Polymeric Chains Combines Effective Target Binding with Long Circulation Times. *Biochim. Biophys. Acta, Biomembr.* **1993**, *1149*, 180–184.
12. Phillips, W. T.; Klipper, R. W.; Awasthi, V. D.; Rudolph, A. S.; Cliff, R.; Kwasiborski, V.; Goins, B. A. Polyethylene Glycol-Modified Liposome-Encapsulated Hemoglobin: A Long Circulating Red Cell Substitute. *J. Pharmacol. Exp. Ther.* **1999**, *288*, 665–670.
13. Wang, C.; Chen, J.; Talavage, T.; Irudayaraj, J. Gold Nanorod/Fe_3O_4 Nanoparticle "Nano-Pearl-Necklaces" for Simultaneous Targeting, Dual-Mode Imaging, and Photothermal Ablation of Cancer Cells. *Angew. Chem., Int. Ed.* **2009**, *121*, 2797–2801.
14. Zhang, G.; Yang, Z.; Lu, W.; Zhang, R.; Huang, Q.; Tian, M.; Li, L.; Liang, D.; Li, C. Influence of Anchoring Ligands and Particle Size on the Colloidal Stability and *in Vivo* Biodistribution of Polyethylene Glycol-Coated Gold Nanoparticles in Tumor-Xenografted Mice. *Biomaterials* **2009**, *30*, 1928–1936.
15. Dreaden, E. C.; Mwakwari, S. C.; Austin, L. A.; Kieffer, M. J.; Oyelere, A. K.; El-Sayed, M. A. Small Molecule-Gold Nanorod Conjugates Selectively Target and Induce Macrophage Cytotoxicity Towards Breast Cancer Cells. *Small* **2012**, *8*, 2819–2822.
16. Bartneck, M.; Keul, H. A.; Zwadlo-Klarwasser, G.; Groll, J. R. Phagocytosis Independent Extracellular Nanoparticle Clearance by Human Immune Cells. *Nano Lett.* **2009**, *10*, 59–63.
17. Salem, A. K.; Searson, P. C.; Leong, K. W. Multifunctional Nanorods for Gene Delivery. *Nat. Mater.* **2003**, *2*, 668–671.
18. Pasut, G.; Veronese, F. M. Peg Conjugates in Clinical Development or Use as Anticancer Agents: An Overview. *Adv. Drug Delivery Rev.* **2009**, *61*, 1177–1188.

19. Chapman, A. P. Pegylated Antibodies and Antibody Fragments for Improved Therapy: A Review. *Adv. Drug Delivery Rev.* **2002**, *54*, 531–545.
20. Bandyopadhyay, A.; Fine, R. L.; Demento, S.; Bockenstedt, L. K.; Fahmy, T. M. The Impact of Nanoparticle Ligand Density on Dendritic-Cell Targeted Vaccines. *Biomaterials* **2011**, *32*, 3094–3105.
21. Haun, J. B.; Hammer, D. A. Quantifying Nanoparticle Adhesion Mediated by Specific Molecular Interactions. *Langmuir* **2008**, *24*, 8821–8832.
22. Fakhari, A.; Baoum, A.; Siahaan, T. J.; Le, K. B.; Berkland, C. Controlling Ligand Surface Density Optimizes Nanoparticle Binding to Icam-1. *J. Pharm. Sci.* **2011**, *100*, 1045–1056.
23. Waite, C. L.; Roth, C. M. Binding and Transport of Pamam-Rgd in a Tumor Spheroid Model: The Effect of Rgd Targeting Ligand Density. *Biotechnol. Bioeng.* **2011**, *108*, 2999–3008.
24. Arnida; Janát-Amsbury, M. M.; Ray, A.; Peterson, C. M.; Ghandehari, H. Geometry and Surface Characteristics of Gold Nanoparticles Influence Their Biodistribution and Uptake by Macrophages. *Eur. J. Pharm. Biopharm.* **2011**, *77*, 417–423.
25. Sheng, K. C.; Kalkanidis, M.; Pouniotis, D. S.; Esparon, S.; Tang, C. K.; Apostolopoulos, V.; Pietersz, G. A. Delivery of Antigen Using a Novel Mannosylated Dendrimer Potentiates Immunogenicity *in Vitro* and *in Vivo*. *Eur. J. Immunol.* **2008**, *38*, 424–436.
26. Inaba, K.; Inaba, M.; Romani, N.; Aya, H.; Deguchi, M.; Ikehara, S.; Muramatsu, S.; Steinman, R. M. Generation of Large Numbers of Dendritic Cells from Mouse Bone Marrow Cultures Supplemented with Granulocyte/Macrophage Colony-Stimulating Factor. *J. Exp. Med.* **1992**, *176*, 1693–1702.
27. Joubert, L. M. Scanning Electron Microscopy: Bridging the Gap from Stem Cells to Hydrogels. *Microsc. Microanal.* **2010**, *16*, 596–597.
28. Cruz, L. J.; Tacken, P. J.; Fokkink, R.; Joosten, B.; Stuart, M. C.; Albericio, F.; Torensma, R.; Figdor, C. G. Targeted Plga Nano- but Not Microparticles Specifically Deliver Antigen to Human Dendritic Cells *via* Dc-Sign *in Vitro*. *J. Controlled Release* **2010**, *144*, 118–126.
29. Steenblock, E. R.; Fadel, T.; Labowsky, M.; Pober, J. S.; Fahmy, T. M. An Artificial Antigen-Presenting Cell with Paracrine Delivery of Il-2 Impacts the Magnitude and Direction of the T Cell Response. *J. Biol. Chem.* **2011**, *286*, 34883–34892.
30. Hamdy, S.; Haddadi, A.; Shayeganpour, A.; Samuel, J.; Lavasanifar, A. Activation of Antigen-Specific T Cell-Responses by Mannan-Decorated Plga Nanoparticles. *Pharm. Res.* **2011**, *28*, 2288–2301.
31. Metaferia, B. B.; Rittler, M.; Gheeya, J. S.; Lee, A.; Hempel, H.; Plaza, A.; Stetler-Stevenson, W. G.; Bewley, C. A.; Khan, J. Synthesis of Novel Cyclic Ngr/Rgd Peptide Analogs Via on Resin Click Chemistry. *Bioorg. Med. Chem. Lett.* **2010**, *20*, 7337–7340.